Supporting information

Modulating intermolecular interactions by collaborative material design to realize THF-processed organic photovoltaic with 1.3 V open-circuit voltage

*Tingting Dai[1,2‡], Ailing Tang[1‡], Zehua He[1,3], Mengzhen Du[1,3], Peng Lei[1], Qingdao Zeng[1], Zongtao Wang[1,3], Yuheng Wang[4], Shirong Lu[5], Yufei Zhong[6], Erjun Zhou[*1, 2]*

[1] CAS Center for Excellence in Nanoscience, National Center for Nanoscience and Technology, Beijing 100190, China.

[2] Center of Materials Science and Optoelectronics Engineering, University of Chinese Academy of Sciences, Beijing 100049, China.

[3] Henan Institute of Advanced Technology, Zhengzhou University, Zhengzhou 450003, China.

[4] Faculty of Electrical Engineering and Computer Science, Ningbo University, Ningbo 315211, Zhejiang, China.

[5] Department of Material Science and Technology, Taizhou University, Taizhou 318000, Zhejiang, China.

[6] School of Materials Science and Engineering, NingboTech University, Ningbo 315100, China.

E-mail: zhouej@nanoctr.cn

[‡] *These two authors contributed equally to this work*

Experiment Section

Measurements and characterizations

^{1}H NMR (400 MHz) weas recorded with a Bruker AVANCE 400 spectrometer in deuterated dichloromethane ($CDCl_3$) and 1,2-dichlorobenzene ($C_2D_4Cl_2$). Chemical shifts are given in ppm units using tetramethylsilane (TMS) as an internal standard. Molecular weights of the polymers were measured on Angilent Technologies PL-GPC 220 high-temperature-chromatograph at 150 °C using a calibration curve of polystyrene standards and 1,2,4-trichlorobenzene as the eluent. Thermo gravimetric analysis (TGA) was recorded on Diamond TG/DTA under the protection of nitrogen at a heating rate of 10 °C/minute. Differential scanning calorimetry (DSC) was performed using a TA DSC Q2000 instrument under nitrogen at the heating and cooling rates of 10 °C/min in one heating/cooling cycles. UV-vis spectra were measurement with a Lambda 950 spectrophotometer. Electrochemical CV was performed on an electrochemical workstation (Chenhua, Shanghai) with a Pt disk coated with a molecular film, a Pt wire, and an Ag/AgCl electrode acting as the working, counter, and reference electrodes, respectively, in a 0.1 mol/L tetrabutylammonium phosphorus hexafluoride (Bu_4NPF_6) acetonitrile solution. AFM height images were obtained on a Multimode 8HR at the tapping mode. The morphologies of the nanostructures were characterized by transmission electron microscopy (TEM, Tecnai G2 F20 U-TWIN, FEI Co., USA). The thickness of the active layer was tested on a Kla-TencorAlpha-StepD-120 Stylus Profiler. The films used for various characterizations were prepared from THF.

The Measurement of Carrier Mobilities

The carrier mobilities of the polymer was investigated by the space charge limited current (SCLC) method. The hole mobility of the blend films was measured with the device structure of ITO/PEDOT: PSS/active layer /Au (80 nm), while the electron mobility of the blends was tested with the devices structure of ITO/TiO_x/active layer /PFNBr/Al (80 nm).

The SCLC model is described by modified Mott-Gurney law:

$$J = (9/8)\ \varepsilon_0\varepsilon_r\mu(V^2/L^3)$$

where J stands for current density, ε_0 is the permittivity of free space (8.85×10^{-12} C V^{-1} m^{-1}), ε_r is the relative dielectric constant of the transport medium (assuming that of 3.0), μ is the carrier mobility, V is the internal potential in the device and L is the thickness of the active layer. The thickness of active layers based on **BTA3**, **BTA3-4F** and **E18**: **BTA3**/**BTA3-4F** are estimated to be 95, 90, 91 and 94 nm for the electron-only devices and 80, 82, 90 and 91 nm for the hole-only devices, respectively.

***J-V* curves**

The J−V curves were measured in glove box with a Keithley 2420 source measure unit. The photocurrent was obtained under illumination using an Oriel Newport 150W solar simulator (AM 1.5G), and the light intensity was calibrated with a Newport reference detector (Oriel PN 91150 V). The EQE measurements of the devices were performed in air with an Oriel Newport system (Model 66902).

2D-GIWAXS Characterization

Two-dimensional grazing incidence wide angle X-ray scattering (2D-GIWAXS) analyses were investigated at the XEUSS SAXS/WAXS equipment. The data were obtained with an area Pilatus 100k detector with a resolution of 195 × 487 pixels (0.172 mm × 0.172 mm). The X-ray wavelength was 1.54 Å, and the incidence angle was 0.2°. The samples were spin-coated onto the PEDOT: PSS/Si substrate. The samples were prepared with the optimized device fabrication conditions.

Highly sensitive EQE and EQE_{EL} measurements

Highly sensitive EQE was measured using an integrated system (PECT-600, Enlitech), where the photocurrent was amplified and modulated by a lock-in instrument. EQE_{EL} measurements were performed by applying external voltage/current sources through the devices (ELCT-3010, Enlitech). EQE_{EL} measurements were performed for all devices according to the optimal device preparation conditions.

Film-depth-dependent light absorption spectra

Film-depth-dependent light absorption spectroscopy was measured by a homemade setup. Soft plasma generated by low-pressure (less than 20 Pa) oxygen was used for the incremental etching of the organic film. The UV–vis absorption spectrum during each etching was in-situ monitored by an optical spectrometer. Beer–Lambert's law was utilized to fit the film-depth-dependent light absorption spectra, which were subsequently utilized to fit the exciton generation contour upon a modified optical matrix-transfer approach.[1]

Molecular dynamic simulations

Molecular dynamics (MD) simulations[2] were performed using the gromacs 2018. The force field used was OPLS-AA force field.

The BHJ active systems based on **BTA3** and **BTA3-4F** mixed with donor **E18** were simulated by cubic cells, and in each cell, there were 20 polymers and each polymer consists of 5 terpolymer repeating units with 4 repeating unit for the eighth equal and 1 repeating unit for the second equal. The numbers of the acceptor molecules put in the cells were 3 determined from the donor: acceptor weight ratios used for fabricating the corresponding solar cells. The initial simulations were carried out by randomly placing the polymers and the acceptor molecules in the cells with a very low density (0.0997 g cm^{-3}). The corresponding construction process was done using gromacs, and the ring spearing and close contacts were examined with VMD. Then, subsequent MD simulations were performed with the NPT ensemble from 650 K (500 ps) to 450 K (500 ps), and then to 300 K (1 ns) at a pressure of 1 atmosphere (450 K is the temperature used for annealing the active layers of the solar cells). The cooling from 650 K to 450 K was done in five successive NPT simulations (600 K for 100 ps, 550 K for 100 ps, 500 K for 100 ps, 450 K for 100 ps). After the simulation of the annealing process at the 450 K, the cooling from 450 K to 300 K was done in three successive NPT simulations (450 K for 500 ps, 350 K for 500 ps and 300 K for 1 ns). The Nose-Hoover thermostat/barostat was used for controlling the temperature and the pressure. The time step for the NPT simulations was 1 fs, and the cutoff for the summation of

van der Waals interactions was 12.5 Å.

The simulation results for the BHJ solar cells based on the **E18**: **BTA3**/**BTA3-4F** are given in **Figure 3**.

TA spectroscopy

TA spectroscopy was tested by a regenerative amplified Ti: sapphire laser system (Coherent) as the laser source and EOS spectrometer (Ultrafast Systems LLC) as the spectrometer, pump beam excitation intensity at 4 μJ cm^{-2}.

Photovoltaic device fabrication

The OSC devices were constructed with a configuration of ITO/PEDOT: PSS/active layer/PFNBr/ Al. A thin layer of PEDOT: PSS (30 nm, Clevios P VP AI 4083) was spin-casted on pre-cleaned ITO-coated glass at 4000 rpm, 30 s. After baking at 150℃ for 15 min, the substrates were transferred into glovebox. Optimized devices were prepared under the following conditions. The rate of the Donor: Acceptor was 1:1 and dissolved in tetrahydrofuran (THF) with a total concentration of 12 mg/mL for 1 hour at 50℃ and then the active layers was spin-coated from the above solution at 1900 rpm, 30 s. Subsequently, they were separately annealed at 150℃, 10 min for **E18**: **BTA3**/**BTA3-4F**. The thickness of the photoactive layer is in the range of 80−100 nm. The interlayer PFNBr was spin-coated on the top of all active layers at 3000 rpm for 30 s. And the PFNBr was dissolved in methanol at a concentration of 0.5 mg/ml. Finally, Al (80 nm) metal top electrode was thermal evaporated onto the active layer under about 1×10^{-4} Pa. The active area of the device was 0.04 cm^2 defined by shadow mask.

Materials and Synthesis

Materials

All chemicals and solvents were reagent grades, which were purchased from Alfa, ACMEC, Bidepharm, TCI, J&K Scientific, Beijing Chemical Plant or other chemical companies. Chemicals and solvents were used without further purification (unless otherwise noted). And the synthesis of **BTA3** is referred to our previously reported literature.[3]

The synthesis of BTA3-4F

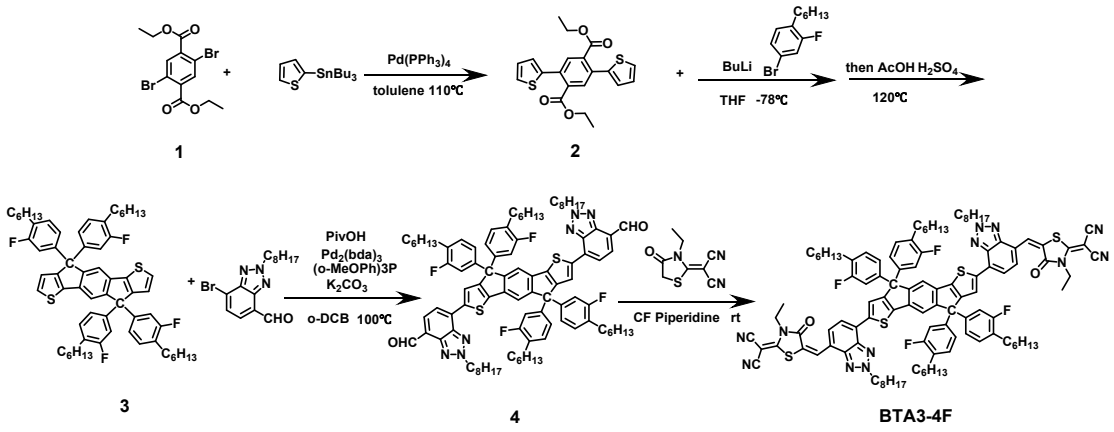

Scheme S1. The synthesis route of nonfullerene acceptor of **BTA3-4F**.

The synthesis of diethyl 2,5-di(thiophen-2-yl) terephthalate compound 2

Diethyl-2,5-dibromoterephthalate (**1**) (5.00 g, 0.013 mol), tributyl(thiophen-2-yl) stannane (14.85 g, 0.040 mol) and catalyst were added to a 100 mL Schlenk flask and then 30 mL toluene was dropped into the flask. The reaction flask was vacuumed, then filled with nitrogen and repeated several times. The reaction flask was then stirred at

110℃ for 24 hours. After the reaction, the solution was cooled to room temperature, the organic phase was extracted with dichloromethane, and the excess solvent was removed by spin evaporation. Crude product was purified by column chromatography using DCM/PE (1:5) as the eluent. Orange solid was obtained with a yield of 90% (4.52 g). ^{1}H NMR (400 MHz, Chloroform-*d*): δ 7.84 (s, 2H), 7.41 (dd, *J* = 4.9, 1.5 Hz, 2H), 7.15 – 7.00 (m, 4H), 4.24 (q, *J* = 7.1 Hz, 4H), 1.18 (t, *J* = 7.1 Hz, 6H).

The synthesis of compound 3:

Compound **2** (0.75 g, 1.94 mmol) was dissolved into 20 mL THF. The solvent was cooled to -78°C and n-butyllithium was added under nitrogen protection. After 1 h stirring, 4-bromo-2-fluoro-1-hexylbenzene (3.02 g, 11.64 mmol) was added into the flask. Then the solvent was warmed naturally to room temperature and reacted overnight. The crude product was extracted with ethyl acetate and proceeded directly to the next step reaction.

The crude product was dissolved into 50 mL acetic acid and then 2.88 mL concentrated sulfuric acid was slowly dropped into the solution. The reaction was stirred 2 h at 120℃, then cooled to room temperature. After extracted with n-hexane and dichloromethane, the excess solvent was removed by spin evaporation. Then the crude product was purified by column chromatography using DCM/PE (1:10) as the eluent. White solid was obtained with a yield of 46.12% (0.88g). ^{1}H NMR (400 MHz, Chloroform-*d*): δ 7.43 (s, 2H), 7.31 (d, *J* = 4.9 Hz, 2H), 7.08 (t, *J* = 8.0 Hz, 4H), 7.01 (d, *J* = 4.9 Hz, 2H), 6.98 – 6.82 (m, 8H), 2.59 (t, *J* = 7.8 Hz, 8H), 1.68 – 1.49 (m, 9H),

1.43 – 1.20 (m, 24H).

The synthesis of compound 4:

Compound **3** (210.0 mg, 0.20 mmol), trimethylacetic acid (10.2 mg, 0.10 mmol), potassium carbonate (138.2 mg, 1.00 mmol), Pd2(bda)3 (9.2 mg, 0.01 mmol), (o-MeOPh)$_3$P (16.2 mg, 0.02 mmol) and 7-bromo-2-octyl-2H-benzo[d][1,2,3]triazole-4-carbaldehyde (161.6 mg, 0.48 mmol) were dissolved in 2.0 mL o-DCB. Then the mixture was protected by nitrogen gas and stirred at 100℃ for 24 h. After cooled down to room temperature, the extra solvent was removed. And the crude product was extracted with chloroform, and purified by column chromatography using EA/PE (1:20) as the eluent. Red solid was obtained with a yield of 90% (268.7 mg). ^{1}H NMR (400 MHz, Chloroform-*d*): δ 10.42 (s, 2H), 8.14 (s, 2H), 7.97 (d, *J* = 7.6 Hz, 2H), 7.80 (d, *J* = 7.6 Hz, 2H), 7.56 (s, 2H), 7.15 (t, *J* = 8.0 Hz, 4H), 7.11 – 6.99 (m, 8H), 4.89 (t, *J* = 7.4 Hz, 4H), 2.62 (t, *J* = 7.8 Hz, 8H), 2.21 (q, *J* = 7.3 Hz, 4H), 1.61 (t, *J* = 7.7 Hz, 9H), 1.44 – 1.37 (m, 10H), 1.31 (dd, *J* = 10.1, 6.3 Hz, 29H), 0.88 (td, *J* = 6.7, 3.5 Hz, 18H).

The synthesis of BTA3-4F

Compound 4 (250.0 mg, 0.17 mmol) and 2-(3-ethyl-4-oxothiazolidin-2-ylidene) malononitrile (77.6 mg, 0.40 mmol) were dissolved into chloroform under the protection of nitrogen. Then piperidine (0.10 ml) was added into the mixture by syringe. After stirred at room temperature for 4 h, the reaction was quenched by water. And the crude product was extracted with chloroform, and purified by column chromatography

using DCM/PE (1:1) as the eluent. Black solid was obtained with a yield of 70% (219.5 mg). ^{1}H NMR (400 MHz, Chloroform-*d*): δ 8.36 (s, 2H), 8.10 (s, 2H), 7.75 (d, *J* = 7.8 Hz, 2H), 7.59 (d, *J* = 7.9 Hz, 2H), 7.55 (s, 2H), 7.15 (t, *J* = 7.9 Hz, 4H), 7.10 – 6.89 (m, 8H), 4.86 (t, *J* = 7.1 Hz, 4H), 4.38 (q, *J* = 7.1 Hz, 4H), 2.62 (t, *J* = 7.9 Hz, 8H), 2.30 – 2.20 (m, 4H), 1.62 (q, *J* = 7.4 Hz, 6H), 1.50 – 1.18 (m, 40H), 0.96 – 0.79 (m, 15H). ^{13}C NMR (101 MHz, Chloroform-d) δ 166.77, 166.66, 162.26, 159.82, 143.27, 143.20, 142.43, 132.20, 131.31, 130.69, 130.63, 128.90, 128.73, 124.35, 123.41, 123.38, 121.60, 121.34, 118.00, 117.73, 115.08, 114.84, 113.23, 62.73, 57.32, 55.25, 40.53, 31.72, 31.63, 30.07, 29.79, 29.72, 29.16, 29.07, 28.90, 28.79, 26.55, 22.60, 22.57, 14.19, 14.07. Element analysis: Anal. calcd. for $C_{110}H_{118}F_4N_{12}O_2S_4$: C 71.63, H 6.45, N 9.11. Found: C 71.44, H 6.38, N 9.15.

The synthesis of E18

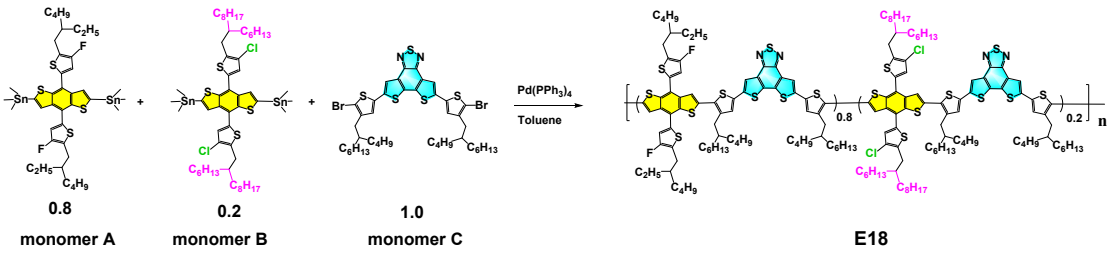

Scheme S2. The synthesis route of **E18**.

Monomer **A** (150.5 mg, 0.16 mmol), monomer **B** (47.9 mg, 0.04 mmol), monomer **C** (181.4 mg, 0.20 mmol) were dissolved in ultra-dry toluene (14 mL) with a 50 mL Schlenk flask. The mixture was purged by nitrogen for 15 min, then $Pd(PPh_3)_4$ (11.6

mg) was added as catalyst, and the mixture was purged by nitrogen for another 15 min. The mixture was heated to 110 °C for 48 h. After cooling, the mixture was precipitated into methanol. The raw polymer was put in Soxhlet extraction and extracted with methanol, hexane and chloroform. The resulted chloroform fraction was precipitated in methanol. Then the precipitate was collected to give **E18** as black solid with a yield of 97% (274.0 mg).^{1}H NMR ($CDCl_3$, 400 MHz, δ/ppm): 7.0 (br, aromatic protons), 2.9 (br, aliphatic protons), 0.7-1.8 (br, aliphatic protons).

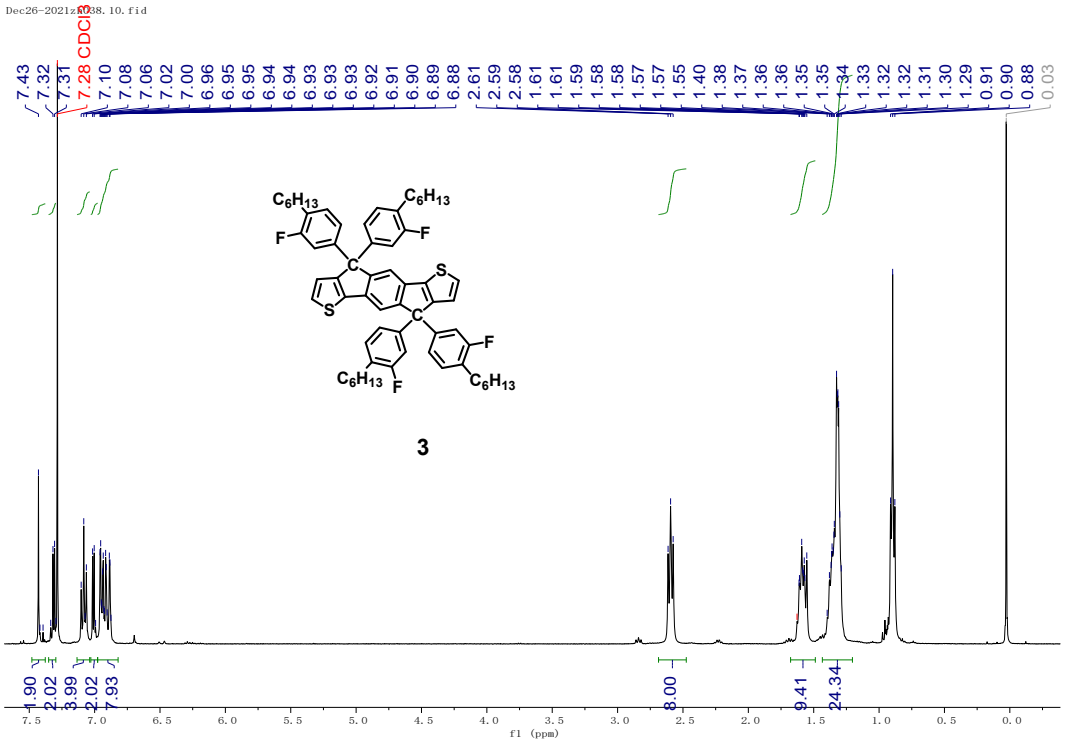

Figure S1 . ^{1}H NMR spectrum of compound **3** at room temperature (400 MHz, Chloroform-*d*).

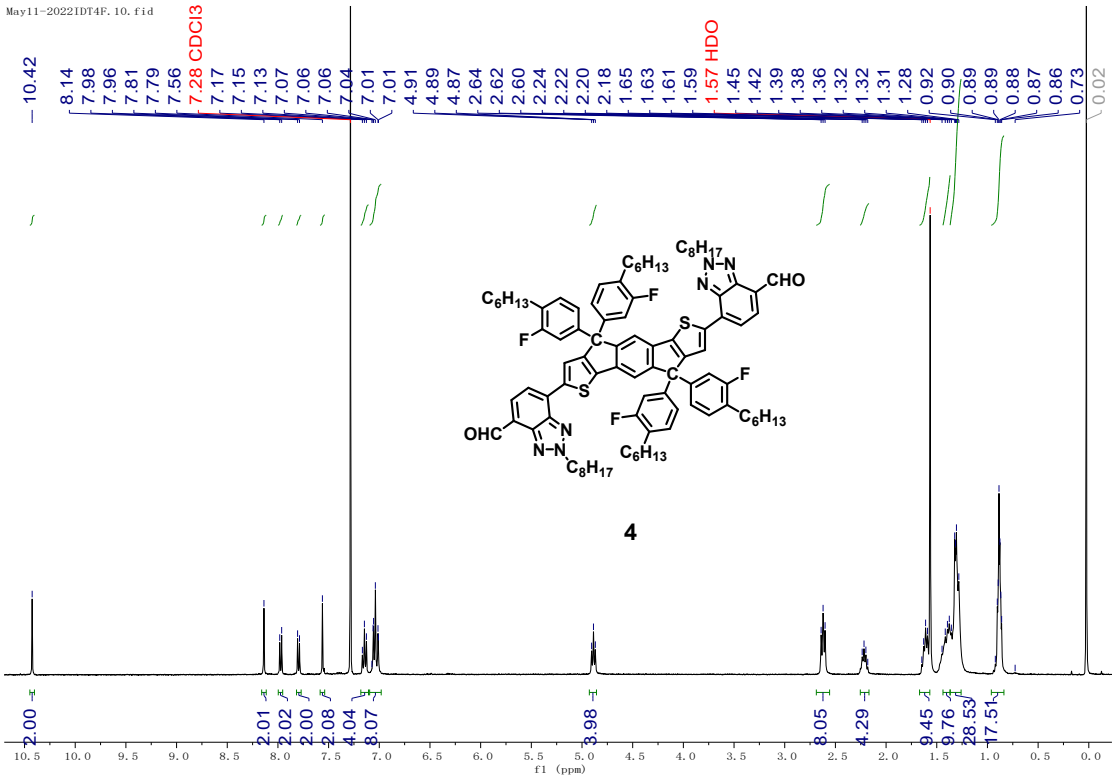

Figure S2. ^{1}H NMR spectrum of compound **4** at room temperature (400 MHz, Chloroform-*d*).

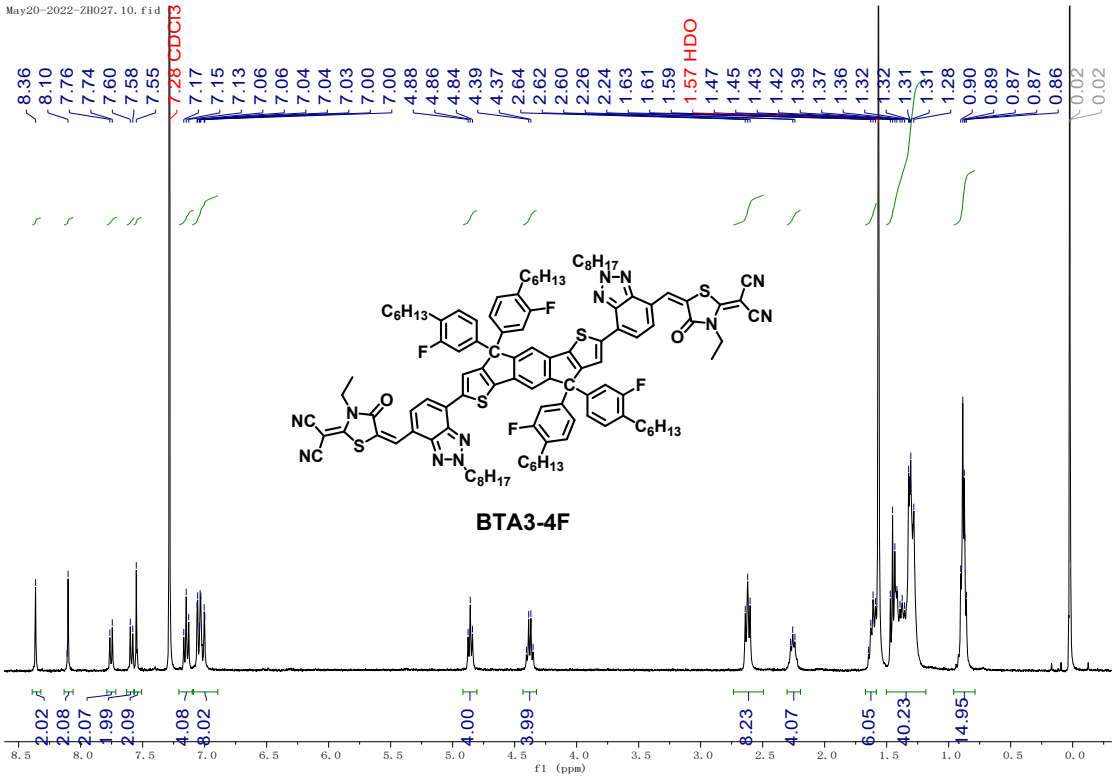

Figure S3. ^{1}H NMR spectrum of **BTA3-4F** at room temperature (400 MHz, Chloroform-*d*).

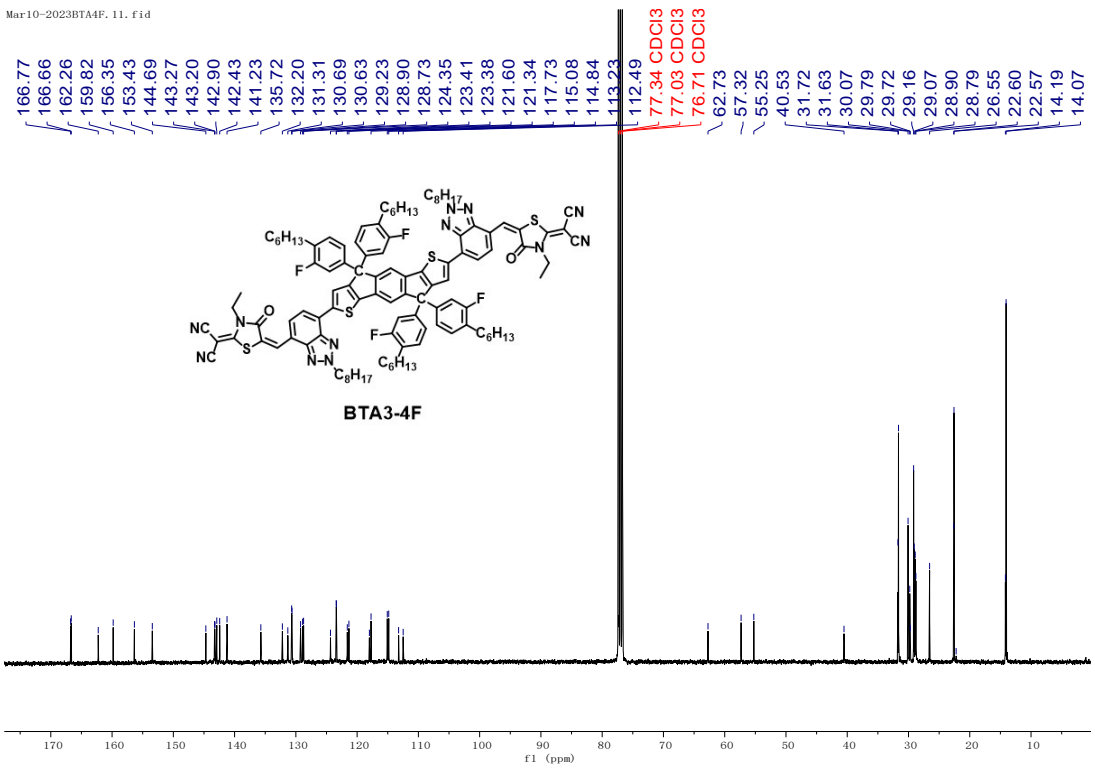

Figure S4. ^{13}C NMR spectrum of **BTA3-4F** at room temperature (101 MHz, Chloroform-*d*).

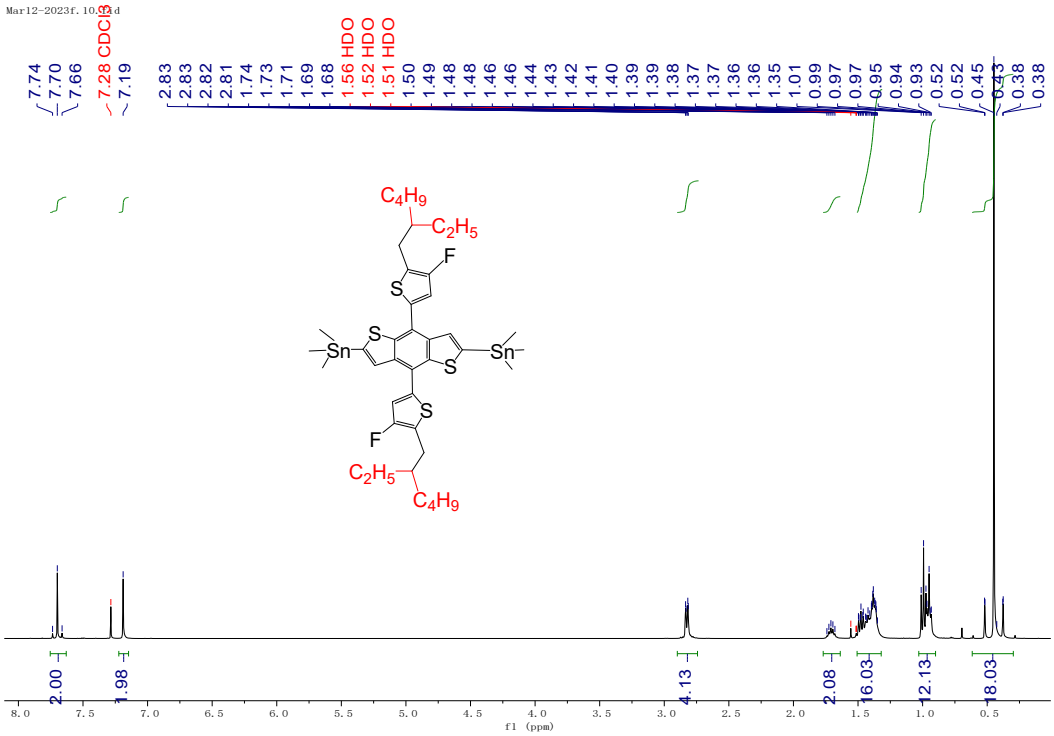

Figure S5. ^{1}H NMR spectrum of monomer A at room temperature (400 MHz, Chloroform-*d*).

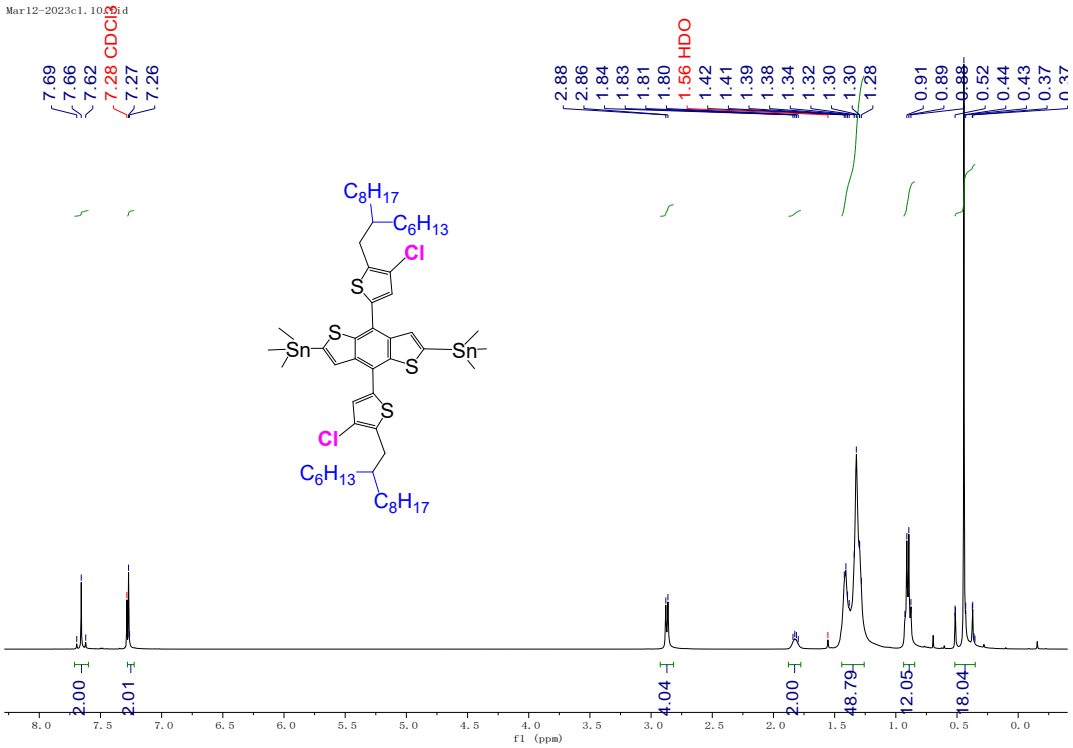

Figure S6. ^{1}H NMR spectrum of monomer B at room temperature (400 MHz, Chloroform-*d*).

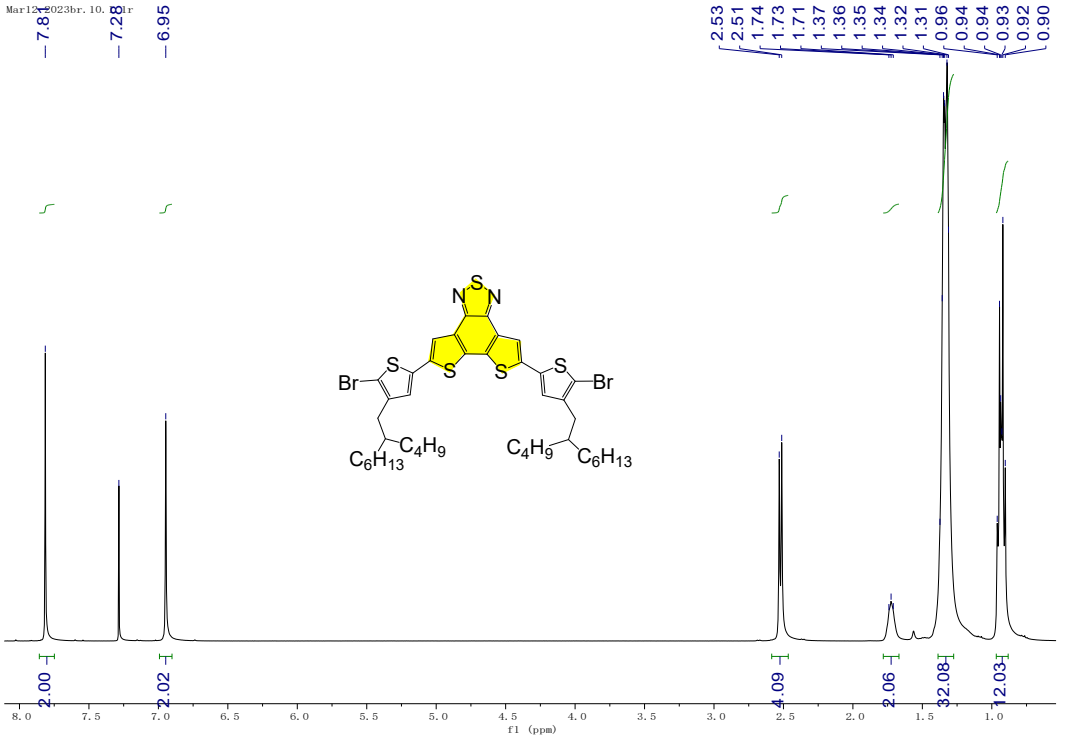

Figure S7. ^{1}H NMR spectrum of monomer C at room temperature (400 MHz, Chloroform-*d*).

Other Figures and Tables:

Table S1. The photovoltaic performance of organic solar cells with $V_{OC} \geq 1.3$ V.

OSCs	V_{OC} (V)	PCE (%)	J_{SC} (mA cm^{-2})	FF	References
J52:ITCCM-O	**1.34**	5.50	9.23	0.44	[4]
P3HT:F8TBT	**1.35**	1.87	3.29	0.42	[5]
PCDTBT:P-BNBP-T	**1.30**	3.20	5.41	0.46	[6]
PTZ1:PMI-F-PMI	**1.30**	6.00	7.00	0.64	[7]
P3HT:BTA100	**1.34**	1.04	1.65	0.47	[8]
PIDT-DTffBTA:BTA2	**1.37**	0.07	0.21	0.23	[9]
J71:BTA701	**1.32**	0.07	0.21	0.25	[10]
D18:PMI-FF-PMI	**1.41**	5.34	6.09	0.61	[11]
PBTT-C4:**BTA3**	**1.32**	3.96	5.83	0.51	[12]
P3HT:PFDTBT-OC6	**1.36**	1.80	2.93	0.45	[13]
PCz:EV-BT	**1.36**	0.75	1.14	0.49	[14]
PCDTBT-C12:SM1	**1.36**	0.59	1.82	0.24	[15]
J52-Cl:BTA1	**1.33**	0.62	1.50	0.31	[16]
PCDTBT-C12:NI-T-NI	**1.30**	2.01	2.91	0.53	[17]
P3HT:PF12TBT	**1.31**	0.91	2.02	0.35	[18]
E18:BTA3	**1.32**	4.98	6.39	0.59	This work
E18:**BTA3-4F**	**1.30**	10.03	11.22	0.69	

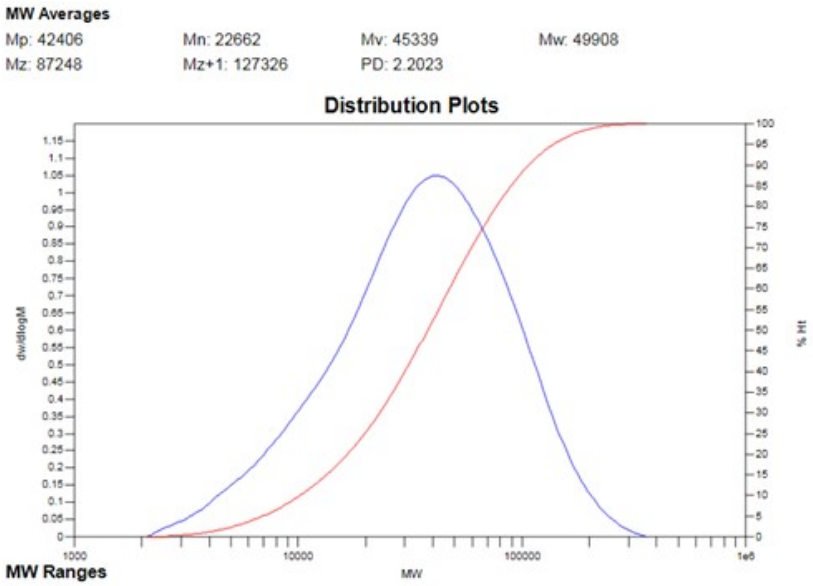

Figure S8.The GPC curves of copolymers **E18**.

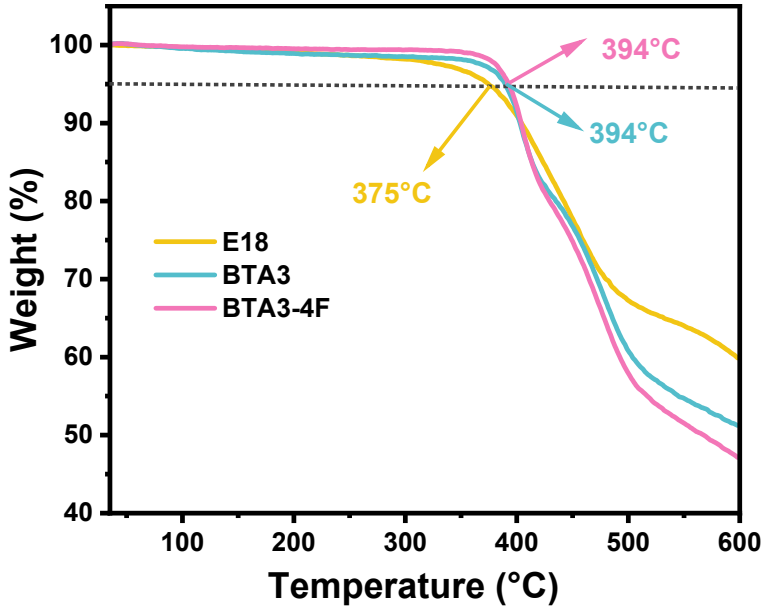

Figure S9. TGA curves of donor and acceptors with a scanning rate of 10°C min^{-1} under an atmosphere of N_2.

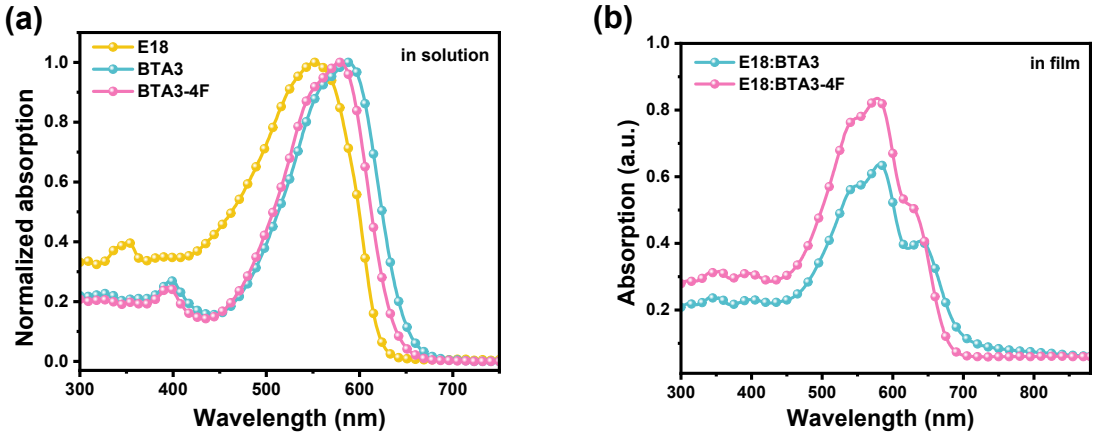

Figure S10. Normalized UV-vis absorption spectra of the relevant molecules (a) in THF solution and (b) in the blend films processed by THF.

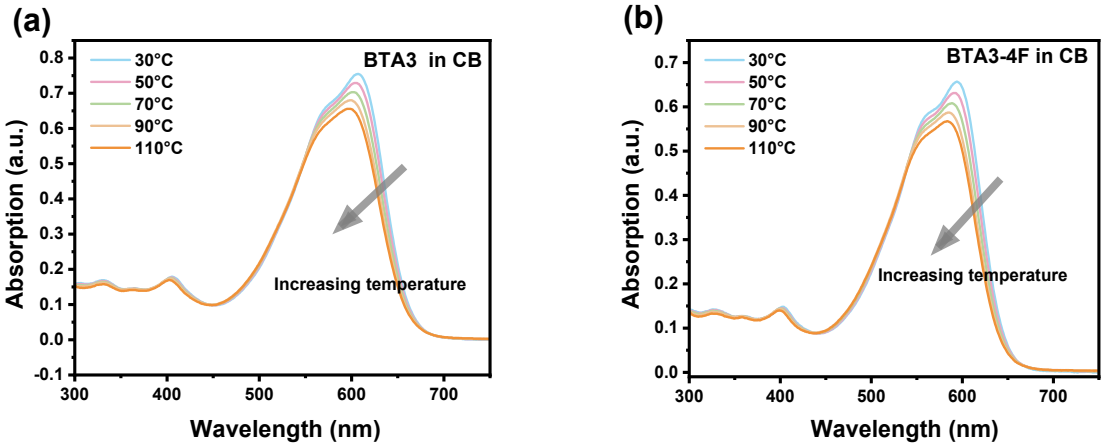

Figure S11. The temperature-dependent absorption spectra in CB (a) for **BTA3** and (b) for **BTA3-4F**.

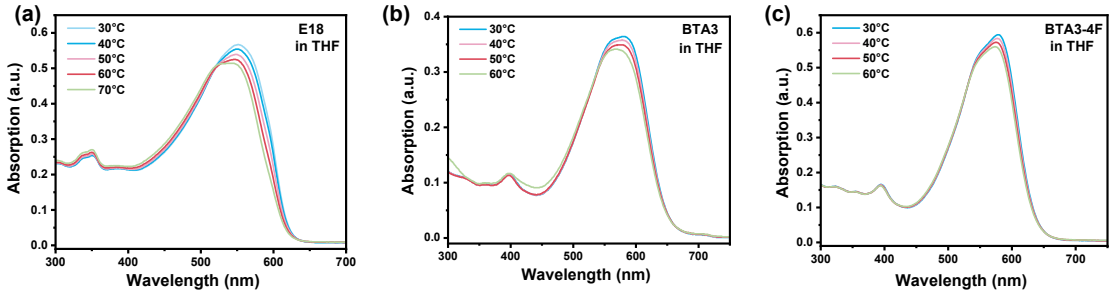

Figure S12. The temperature-dependent UV–vis absorption spectra of the relevant molecules in THF solution (a) for **E18**, (b) for **BTA3** and (c) for **BTA3-4F**.

Table S2. Optical and electrical properties of **E18**, **BTA3** and **BTA3-4F**.

Compounds	$\lambda_{max}^{(sol.)}$ (nm)	$\lambda_{max}^{(film)}$ (nm)	$\lambda_{onset}^{(film)}$ (nm)	E_g^{opt} (eV)[a]	$E_{HOMO}^{(b)}$ (eV)	$E_{LUMO}^{(b)}$ (eV)
E18	552	540	622	1.99	-5.54	-3.64
BTA3	588	585,635	710	1.75	-5.59	-3.71
BTA3-4F	580	580,620	700	1.77	-5.63	-3.74

(a) Calculated from the absorption onset edge of the films, Egopt = 1240/λonset;
(b) obtained from the CV test.

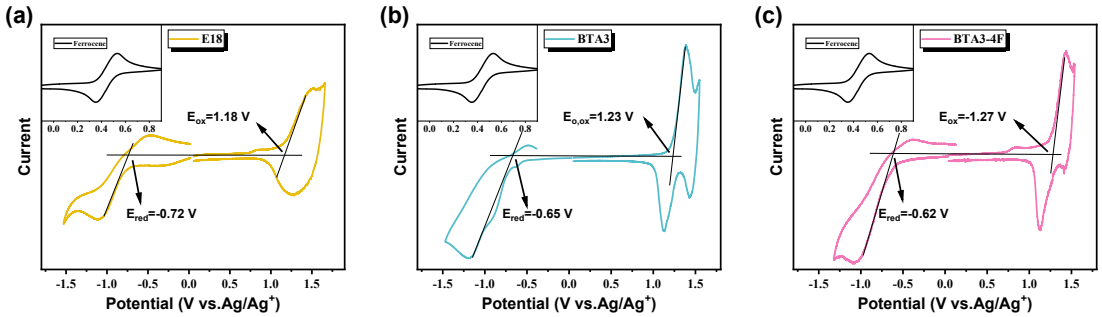

Figure S13. The cyclic voltammogram curves of (a) **E18**, (b) **BTA3** and (c) **BTA3-4F** films on platinum electrodes in acetonitrile solution of 0.1 mol/L Bu_4NPF_6 (Bu = butyl) at a scan rate of 100 mV s^{-1}.

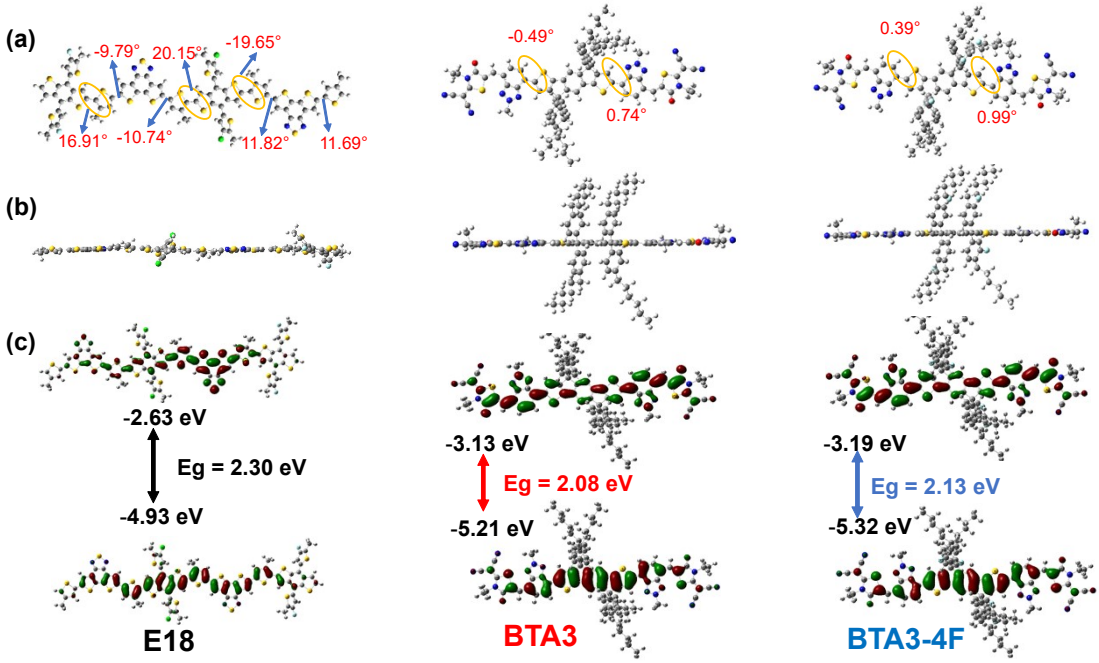

Figure S14. (a) Top view, (b) side view of optimized geometries, and (c) optimized molecular orbitals energy levels for **E18**, **BTA3** and **BTA3-4F** calculated by B3LYP/6-31G (d, p).

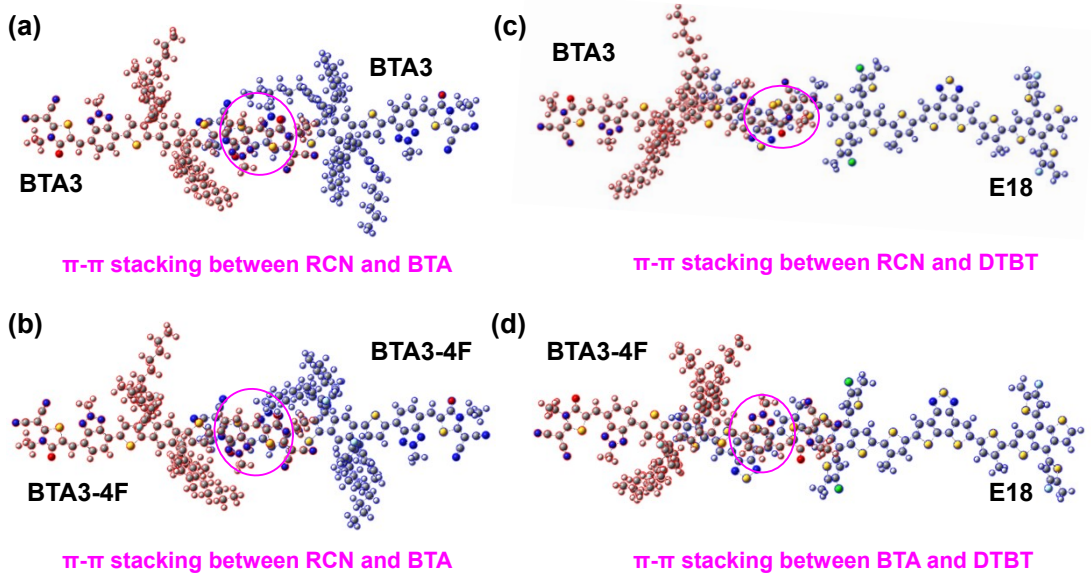

Figure S15. The calculated top view of the optimized intermolecular interactions between acceptors of (a) **BTA3** and (b) **BTA3-4F** or between donor (the bule molecule) and acceptors (the red molecule) of (c) **E18** and **BTA3**, (d) **E18** and **BTA3-4F** based on B3LYP/6-31G (d, p).

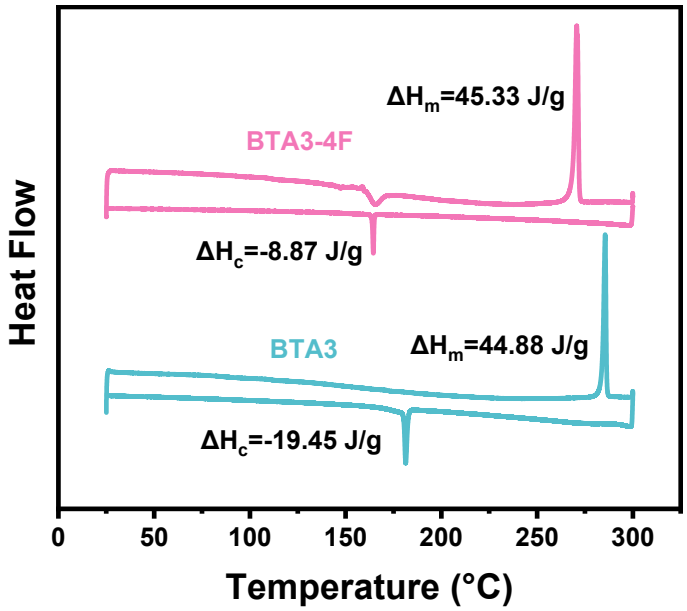

Figure S16. DSC heating and cooling cycles of **BTA3** and **BTA3-4F** in nitrogen atmosphere with a scan rate of 10°C min^{-1}.

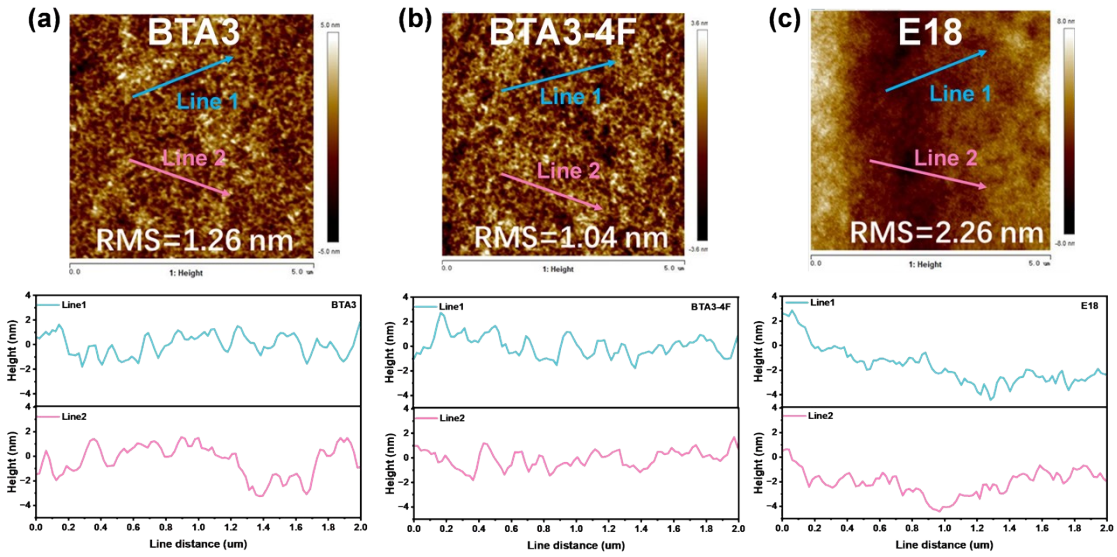

Figure S17. AFM height images (5μm × 5μm) and line profiles of (a) **BTA3**, (b) **BTA3-4F** and (c) **E18**.

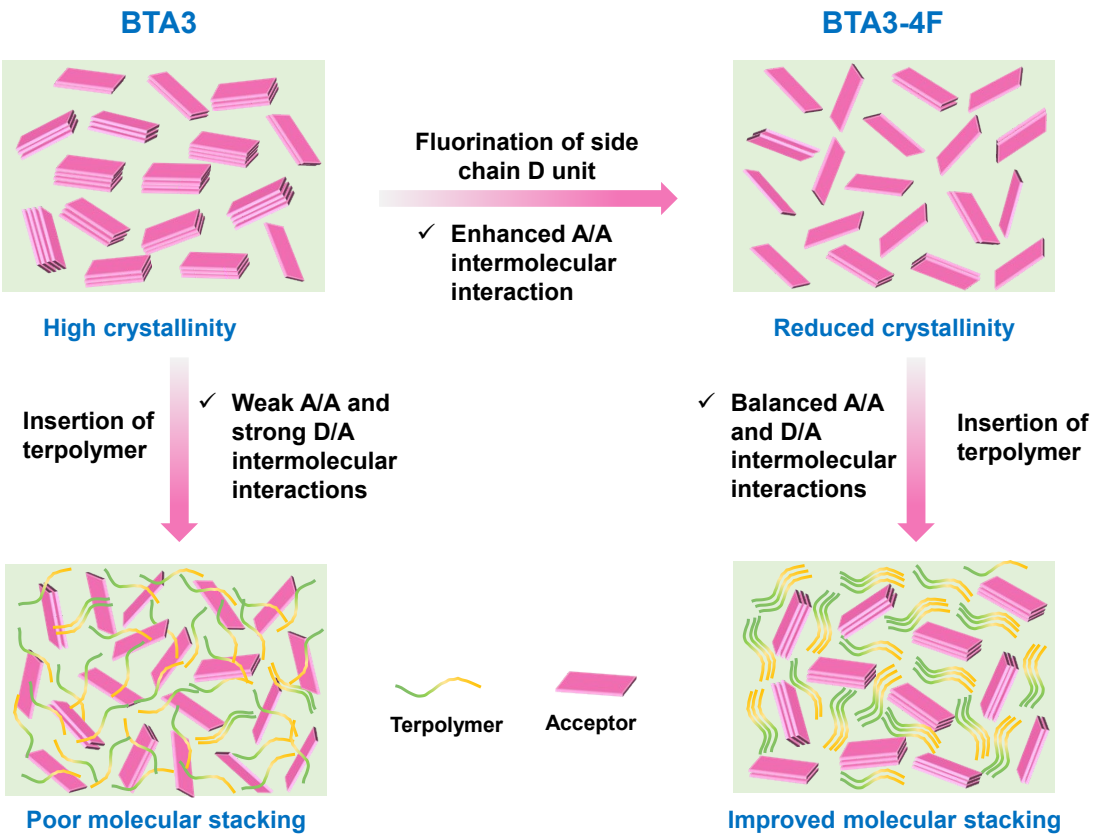

Figure S18. Schematic diagram of the evolution of molecular structure changes and insertion of terpolymer **E18** leading to the different molecule stacking.

Table S3. The photovoltaic performance of **E18: BTA3** and **E18: BTA3-4F** under different donor: acceptor weight ratio processed by THF with thermal annealing at 150°C, 10 min.

Blends	D: A	V_{OC} (V)	J_{SC} (mA/cm^2)	FF (%)	PCE (%)
E18:BTA3	1:1.5	1.312	4.09	50.15	2.86
	1:1	1.317	6.39	58.98	4.98
	1.5:1	1.305	6.03	56.73	4.75
E18:BTA3-4F	1:1.5	1.297	10.39	66.75	8.95
	1:1	1.295	10.94	65.26	9.23
	1.5:1	1.291	11.18	64.15	9.23

Table S4. The photovoltaic performance of **E18: BTA3/BTA3-4F** processed by THF with a D:A weight ratio of 1:1 under different annealing temperature.

Blends	Temperature	V_{OC} (V)	J_{SC} (mA/cm^2)	FF (%)	PCE (%)
E18:BTA3	130℃	1.326	5.54	49.66	3.88
	150℃	1.318	6.01	57.65	4.57
	170℃	1.306	5.43	56.31	4.25
E18:BTA3-4F	130℃	1.300	10.47	61.68	8.40
	140℃	1.297	11.22	68.98	10.03
	150℃	1.293	10.94	65.26	9.23
	170℃	1.278	10.50	69.84	9.35

Table S5. The photovoltaic performance of **E18: BTA3/BTA3-4F** processed by THF with a D:A weight ratio of 1:1 and annealed at 150°C, 10 min, under different additives.

Blends	additives	V_{OC} (V)	J_{SC} (mA/cm^2)	FF (%)	PCE (%)
E18:BTA3	0.5%DPE	1.292	4.66	63.15	4.04
	0.5%DIO	1.295	3.19	54.80	2.41
	0.5%CN	1.310	4.12	55.14	3.16
	/	1.321	6.07	53.44	4.55
E18:BTA3-4F	0.5%DPE	1.289	10.77	66.68	9.30
	0.5%CN	1.291	9.87	68.82	8.81

	0.5%DIO	1.255	5.75	61.48	4.45
	0.5%DMSO	1.092	7.71	42.89	3.63
	3%IPA	1.28	11.27	62.61	9.02
	3%CS_2	1.29	10.11	66.27	8.62
	/	1.288	10.81	67.01	9.38

Table S6. The photovoltaic performance of **E18: BTA3/BTA3-4F** processed by different processing solvents with a D:A weight rations of 1:1 and annealed at 150°C, 10 min,

Blends	**solvents**	V_{OC} **(V)**	J_{SC} **(mA/cm²)**	**FF (%)**	**PCE (%)**
E18:BTA3	THF	1.317	6.39	58.98	4.98
	CF	1.318	5.84	54.16	4.43
	CB	1.325	5.43	49.62	3.80
E18:BTA3-4F	THF	1.297	11.22	68.98	10.03
	CF	1.300	10.25	67.28	8.96
	CB	1.302	9.81	67.96	8.67

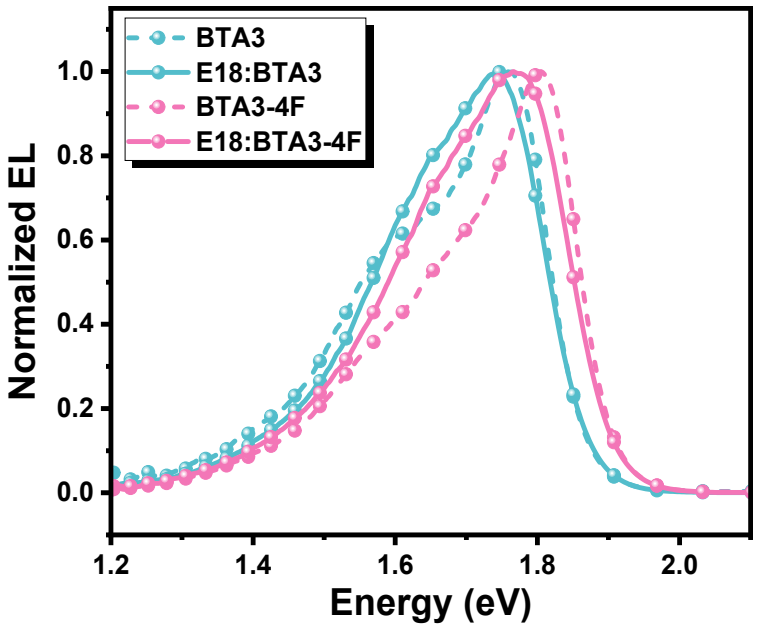

Figure S19. Normalized EL of **BTA3**/**BTA3-4F** and **E18**: **BTA3**/**BTA3-4F** devices.

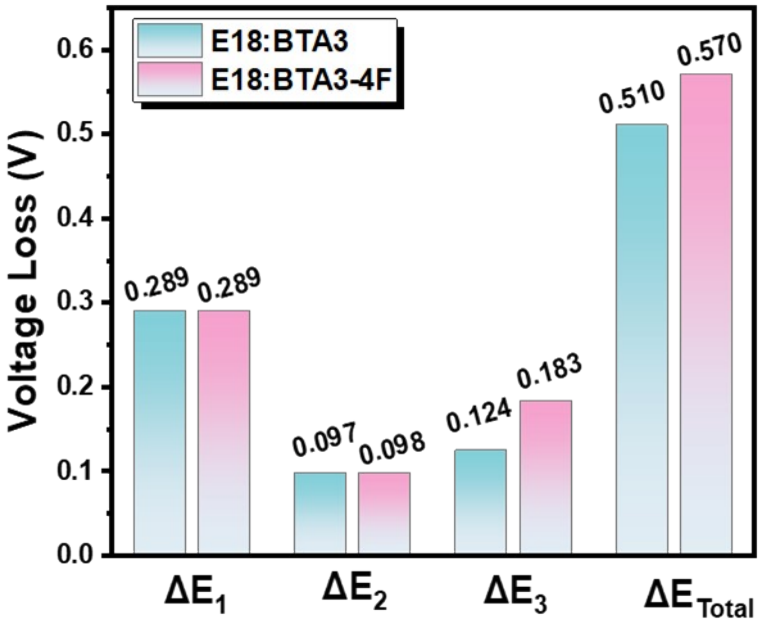

Figure S20. Detailed voltage loss analysis of these devices based on SQ-theory.

Table S7. Detailed energy losses based on the **E18**: **BTA3**/**BTA3-4F** devices based on Shockley-Queisser (SQ) theory.

Blends	E_g^{PV} (eV)	$V_{OC,sq}$ (V)	$V_{OC,rad}$ (V)	$V_{OC,cal}$ (V)	ΔE (eV)	ΔE_1 (eV)	ΔE_2 (eV)	ΔE_3 (eV)	EQE_{EL}(%)
E18:BTA3	1.833	1.544	1.447	1.323	0.510	0.289	0.097	0.124	8.25×10^{-1}
E18:BTA3-4F	1.866	1.577	1.479	1.296	0.570	0.289	0.098	0.183	8.19×10^{-2}

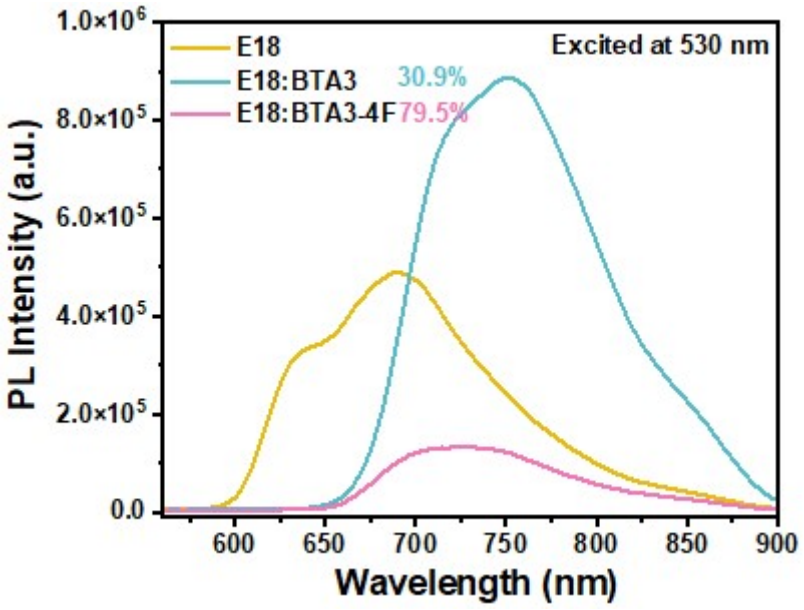

Figure S21. Photoluminescence spectra of the pure donor and their corresponding blend films excited at 530 nm.

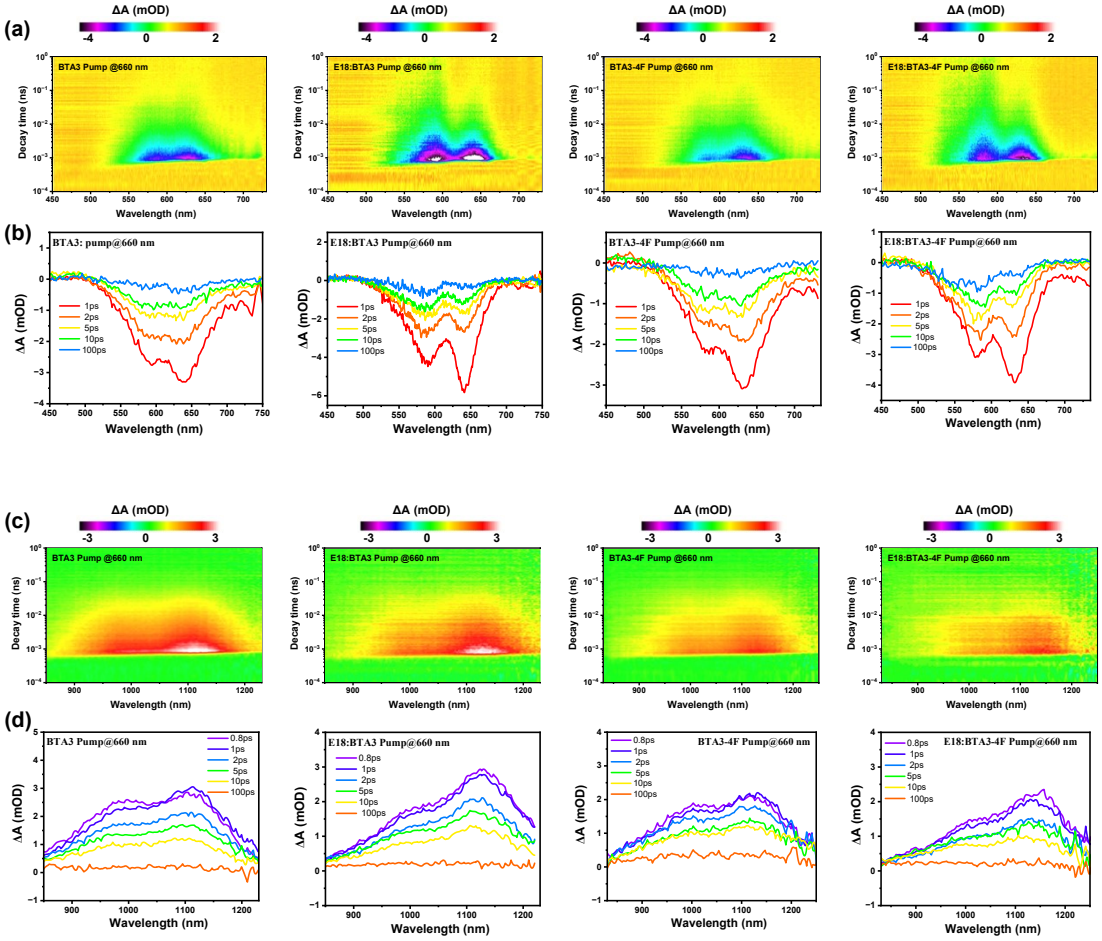

Figure S22. (a, c) The TA signals recorded from the neat **BTA3**/**BTA3-4F** film and its corresponding blend film excited at 660 nm; (b, d) the TA spectra from neat

BTA3/**BTA3-4F** film and its corresponding blend film excited at 660 nm at different delay times.

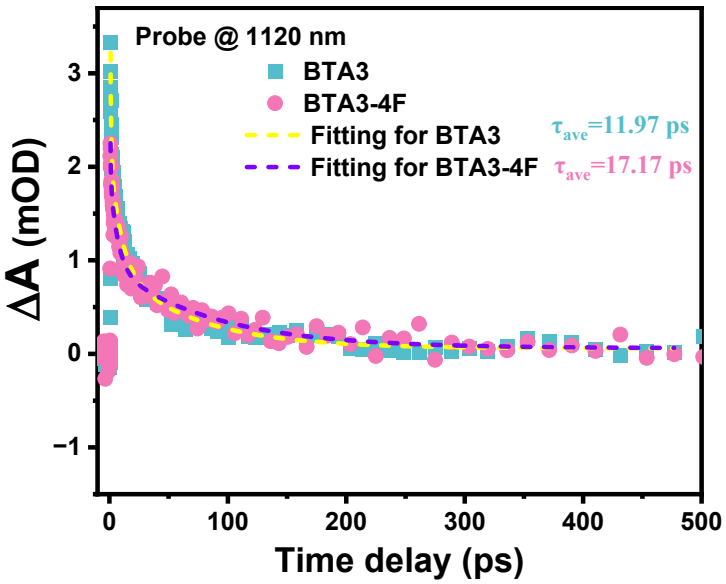

Figure S23. Dynamic fitting of **BTA3**/**BTA3-4F** pure film excited at 660 nm.

Table S8. Summary of decay time of **BTA3**/ **BTA3-4F** neat films and **E18**: **BTA3**/**BTA3-4F** blend films probe at 1120 nm and 1130 nm, respectively, with excited wavelength of 660 nm.

Films	τ_1 (ps)	A1	τ_2 (ps)	A2	τ_3 (ps)	A3	τ_{ave} (ps)
BTA3	0.70±0.09	66%	9.47±1.59	20%	68.66±11.35	14%	11.97
BTA3-4F	0.44 ±0.21	61%	6.39±1.17	21%	86.47±13.21	18%	17.17
E18:**BTA3**	0.74±0.38	42%	5.10±1.40	32%	58.93±8.72	26%	17.26
E18:**BTA3-4F**	0.27 ± 0.13	86%	5.78±1.39	8%	58.06 ± 14.21	6%	4.18

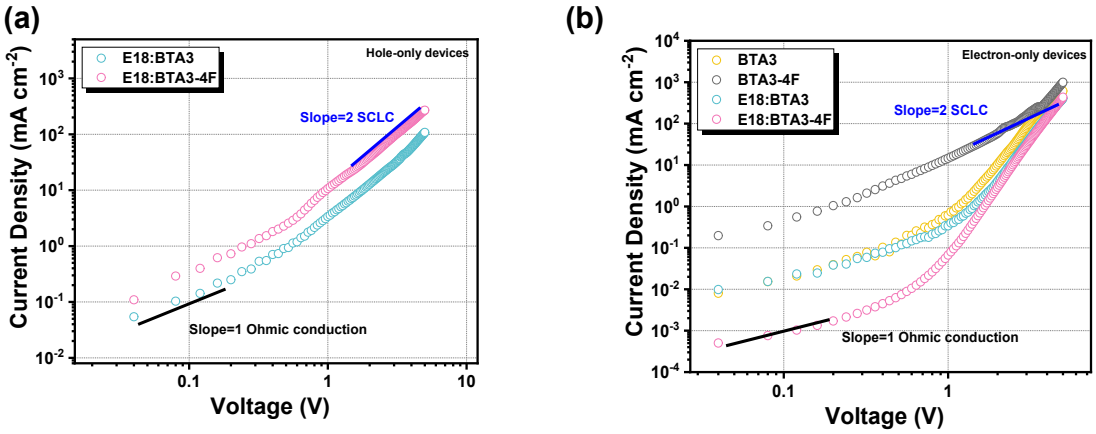

Figure S24. *J-V* curves of the (a) hole-only and (b) electron-only devices.

Reference

1. L. Bu, S. Gao, W. Wang, L. Zhou, S. Feng, X. Chen, D. Yu, S. Li and G. Lu, *Adv. Electron. Mater.* , 2016, **2**, 1600359.
2. J. Wang, X. Jiang, H. Wu, G. Feng, H. Wu, J. Li, Y. Yi, X. Feng, Z. Ma, W. Li, K. Vandewal and Z. Tang, *Nat. Commun.*, 2021, **12**, 6679.
3. X. Wang, A. Tang, J. Yang, M. Du, J. Li, G. Li, Q. Guo and E. Zhou, *Sci. China Chem.* , 2020, **63**, 1666-1674.
4. B. Gao, H. Yao, L. Hong and J. Hou, *Chin. J. Chem.*, 2019, **37**, 1153-1157.
5. W. Yu, D. Yang, X. Zhu, X. Wang, G. Tu, D. Fan, J. Zhang and C. Li, *ACS Appl. Mater. Interfaces*, 2014, **6**, 2350-2355.
6. Z. Ding, X. Long, B. Meng, K. Bai, C. Dou, J. Liu and L. Wang, *Nano Energy*, 2017, **32**, 216-224.
7. Y. Zhang, X. Guo, B. Guo, W. Su, M. Zhang and Y. Li, *Adv. Funct. Mater.*, 2017, **27**, 1603892.
8. Q. Zhang, B. Xiao, M. Du, G. Li, A. Tang and E. Zhou, *J. Mater. Chem. C*, 2018, **6**, 10902-10909.
9. A. Tang, F. Chen, B. Xiao, J. Yang, J. Li, X. Wang and E. Zhou, *Front. Chem.*, 2018, **6**, 147.
10. B. Xiao, Y. Geng, A. Tang, X. Wang, Y. Chen, Q. Zeng and E. Zhou, *Solar RRL*, 2019, **3**, 1800332.
11. J. Hofinger, S. Weber, F. Mayr, A. Jodlbauer, M. Reinfelds, T. Rath, G. Trimmel and M. C. Scharber, *J. Mater. Chem. A*, 2022, **10**, 2888-2906.
12. J. Wang, L. Ma, Y. W. Lee, H. Yao, Y. Xu, S. Zhang, H. Y. Woo and J. Hou, *Chem. Commun.*, 2021, **57**, 9132-9135.
13. Q. Yang, H. Song, B. Gao, Y. Wang, Y. Fu, J. Yang, Z. Xie and L. Wang, *RSC Adv.* , 2014, **4**, 12579-12585.
14. Z. E. Ooi, T. L. Tam, R. Shin, Z. K. Chen, T. Kietzke, A. Sellinger, M. Baumgarten, K. Mullen and J. C. Demello, *J. Mater. Chem.*, 2008, **18**, 4619-4622.

15. J. Zhang, X. Zhang, H. Xiao, G. Li, Y. Liu, C. Li, H. Huang, X. Chen and Z. Bo, *ACS Appl. Mater. Interfaces*, 2016, **8**, 5475-5483.
16. Q. Wu, Y. Yu, X. Xia, Y. Gao, T. Wang, R. Sun, J. Guo, S. Wang, G. Xie, X. Lu, E. Zhou and J. Min, *Joule*, 2022, **6**, 2138-2151.
17. X. Zhang, J. Zhang, H. Lu, J. Wu, G. Li, C. Li, S. Li and Z. Bo, *J. Mater. Chem. C*, 2015, **3**, 6979-6985.
18. M. Osaka, D. Mori, H. Benten, H. Ogawa, H. Ohkita and S. Ito, *ACS Appl. Mater. Interfaces*, 2017, **9**, 15615-15622.